Role of Intrachain Rigidity in the Plasticization of Intrinsically Microporous Triptycene-Based Polyimide Membranes in Mixed-Gas CO 2/CH4 Separations

ARTICLE *in* MACROMOLECULES · OCTOBER 2014

Impact Factor: 5.8 · DOI: 10.1021/ma501798v

5 AUTHORS, INCLUDING:

Raja Swaidan
Air Liquide America
18 PUBLICATIONS **335** CITATIONS
SEE PROFILE

Bader Ghanem
King Abdullah University of Science and Tec…
38 PUBLICATIONS **2,037** CITATIONS
SEE PROFILE

Macromolecules

Article

pubs.acs.org/Macromolecules

Role of Intrachain Rigidity in the Plasticization of Intrinsically Microporous Triptycene-Based Polyimide Membranes in Mixed-Gas CO_2/CH_4 Separations

Raja Swaidan,[†] Bader Ghanem,[†] Majed Al-Saeedi,[‡] Eric Litwiller,[†] and Ingo Pinnau*,[†]

[†]Advanced Membranes and Porous Materials Center (AMPMC), Division of Physical Sciences and Engineering, King Abdullah University of Science and Technology, Thuwal 23955-6900, KSA

[‡]Department of Chemistry, Taibah University, Madinah 30001, KSA

Supporting Information

ABSTRACT: Based on high-pressure pure- and mixed-gas (50:50) CO_2/CH_4 separation properties of two intrinsically microporous triptycene-based polyimides (TPDA−TMPD and TPDA−6FpDA), the intrachain rigidity central to "conventional PIM" design principles is not a singular solution to intrinsic plasticization resistance. Despite the significant intrachain rigidity in TPDA−TMPD, a 300% increase in $P_{MIX}(CH_4)$, 50% decrease in $\alpha(CO_2/CH_4)$ from 24 to 12, and continuous increase in $P_{MIX}(CO_2)$ occurred from 4 to 30 bar. On the other hand, the more flexible and densely packed TPDA−6FpDA exhibited a slight upturn in $P_{MIX}(CO_2)$ at 20 bar similar to a dense cellulose acetate (CA) film, also reported here, despite a 4-fold higher CO_2 sorption capacity. Microstructural investigations suggest that the interconnected O_2- and H_2-sieving ultramicroporosity of TPDA−TMPD is more sensitive to slight CO_2-induced dilations and is the physical basis for a more extensive and accelerated plasticization. Interchain rigidity, potentially by interchain interactions, is emphasized and may be facilitated by intrachain mobility.

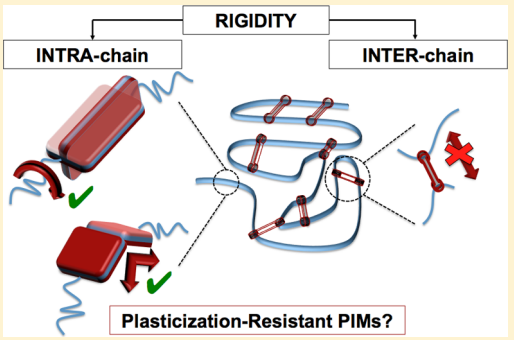

1. INTRODUCTION

Natural gas sweetening is one of the fastest growing industrial applications of polymer membrane-based gas separation technology.[1,2] For almost three decades thin-skinned (~0.1−0.2 μm) asymmetric membranes of glassy cellulosic polymers adopted from reverse osmosis applications have been predominantly used despite their relatively low CO_2 permeabilities and, importantly, high-pressure mixed-gas CO_2/CH_4 selectivities (~10−20). Partly due to CO_2-induced plasticization, low CO_2/CH_4 membrane selectivities result in costly and undesirable copermeation of product CH_4 into the low-pressure CO_2-rich permeate that undermines the competitive position of membrane technology against conventional amine scrubbing.[2,3] To date, its economic viability has been successfully maintained by engineering recycle streams and permeate recompression into two-stage systems that reduce the loss of copermeating product (CH_4). However, great potential for a "game changer" exists in the development of new polymers that are *intrinsically* more selective and resistant to plasticization in the presence of highly condensable feed components like CO_2 and C_{3+} hydrocarbons.

Paramount to addressing plasticization intrinsically through material design is the elucidation of its mechanism. Compelling evidence exists in the macroscopic changes in the bulk physical properties of glassy polymers (e.g., poly(phenylene oxide), polysulfone, poly(ether imide), polycarbonate, cellulose acetate, poly(methyl methacrylate), polyimides) upon exposure to high CO_2 pressures. They include (i) strong depressions (>100 °C) in the glass transition temperature (T_g),[4] (ii) increases in ductility and softness,[5] (iii) increases in the average intersegmental *d*-spacing indicated by WAXD measurements,[6] and (iv) direct observations of volume dilation with increasing partial molar volume of CO_2 via in situ spectroscopic ellipsometry.[7−10] Complementary evidence also exists in the gas transport properties[11−15] of these glassy polymers beyond a certain "plasticization pressure" including (i) pressure-dependent increases in pure CO_2 permeability, increases in mixed-gas CH_4 permeability, and reduction in mixed-gas CO_2/CH_4 selectivity; (ii) time-dependent increases in CO_2 permeability at a given pressure; (iii) concentration-dependent activation energy for diffusion; and (iv) time-dependent sorption. These observations are all consistent with a chain mobilization culminating in a new organizational state over time.[11,12,16]

Accordingly, successful strategies[17,18] that suppress CO_2-induced plasticization are primarily those that restrict chain mobility. They include strong covalent connections between the chains resulting from chemical-cross-linking[19−21] or high-temperature-based cross-linking via polybenzoxazole forma-

Received: August 30, 2014
Revised: October 8, 2014

   dx.doi.org/10.1021/ma501798v | Macromolecules XXXX, XXX, XXX−XXX

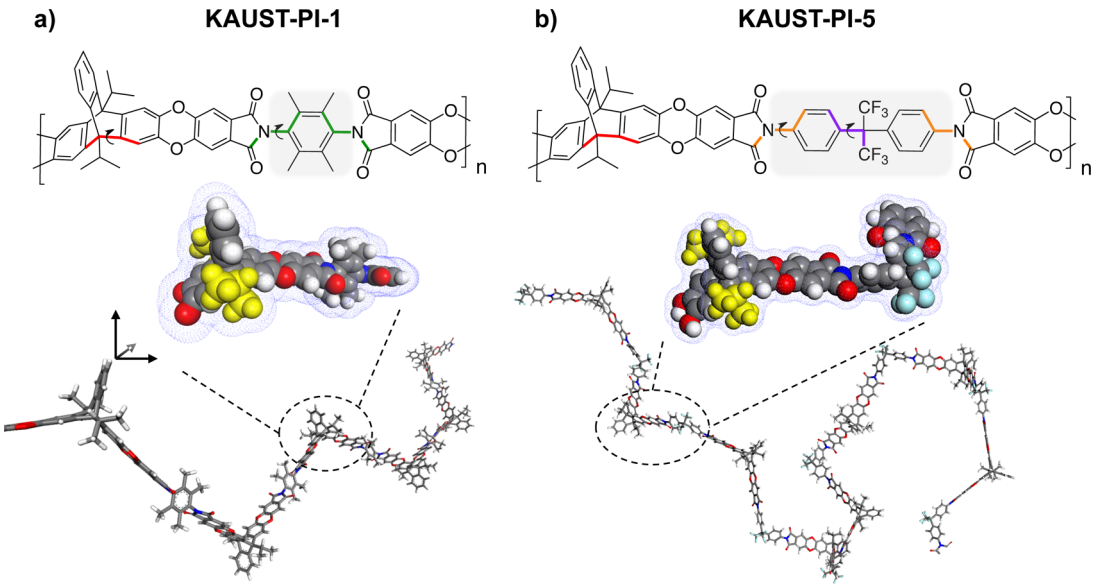

Figure 1. Energy-minimized structures (Forcite module, Materials Studio 7.0, Accelrys) detailing conformational differences in the repeat units and polymer chains of (a) KAUST-PI-1 (TPDA-TMPD) and (b) KAUST-PI-5 (TPDA-6FpDA). Dihedral angle distributions were simulated over the highlighted bonds.

tion[22,23] and pyrolysis.[24−26] They also include increasing interchain interactions via the formation of charge transfer complexes (CTCs) in polyimides and polyamide−imides[27−32] and the integration of polar moieties that engage in strong hydrogen bonding increasing the cohesive energy density (CED) of the microstructure.[31−36] There has been interesting and insightful discussion with regards to the introduction of polar moieties. Puleo et al. argued that higher degrees of acetylation in CA result in easier disruption of chain−chain interactions by CO_2, permitting swelling of the microstructure.[37] This was rationalized by the replacement of strong hydroxyl−hydroxyl interactions with weaker hydroxyl−acetyl and acetyl−acetyl interactions due to the dipolar nature of the carbonyl group.[38] Sanders et al. observed that highly sorbing CO_2 plasticized PMMA but that C_2H_4—which also sorbed significantly—did not.[15] This demonstrated that the magnitude of gas sorption alone could not explain plasticization of permeation properties. As in the case of CA, it was again rationalized through the disruption of weak dipole−dipole interactions between carbonyl groups by the quadrupolar CO_2 molecule, independently confirmed by high-pressure FT-IR studies.[39]

On the other hand, researchers[17,18,40] have speculated about the plasticization resistance of an emerging class of solution-processable materials known as polymers of intrinsic microporosity (PIMs) given their highly restricted intrachain mobility.[41−44] PIMs comprise fused-ring and contorted backbones that pack inefficiently in the solid state to trap microporosity. They often show no T_g below their decomposition temperatures and tend to exhibit lower mechanical flexibility. Significant enhancements in their intrachain rigidities have been accomplished via a fused-ring integration of bridged-bicyclic contortion centers such as ethanoanthracene, Tröger's base, and triptycene.[45−50] The resulting materials, which include ladder polymers[45,49,50] and PIM-type polyimides (PIM-PIs)[46,47,51] have been cast into dense membranes exhibiting remarkable combinations of high permeabilities and high selectivities significantly transcending the latest 2008 upper bounds[52] for O_2 and H_2 separations. However, their rational design disregards interchain rigidity, which appears important for plasticization resistance given the discussion above. Additionally, their high microporosities result in high sorption capacities that have been cautioned against in the selection of membranes for feeds containing condensable components like CO_2.[53] We have recently addressed the pure- and mixed-gas CO_2/CH_4 separation performance of the prototypical PIM, PIM-1.[34] Although no upturns occurred in the pure-gas CO_2 permeability isotherm up to 10 bar, the mixed-gas CH_4 permeability increased more than 60% over the pure-gas values up to 20 bar in a 50:50 CO_2:CH_4 mixture. This plasticization was largely mitigated when the backbone of PIM-1 was functionalized with amidoxime moieties (AO-PIM-1), which, although bulky, engage in interchain hydrogen bonding. Similarly, TZ-PIMs containing hydrogen-bonding tetrazole moieties exhibited enhanced blocking of N_2 transport by CO_2 in the mixed gas, which we hypothesize is due to a tightened and more selective microstructure analogous to that in AO-PIM-1.[34,54] These results again suggest that interchain rigidity is paramount to the intrachain rigidity in maintaining selective performance under aggressive CO_2/CH_4 mixed-gas feeds. Additionally, these experiments emphasize that only mixed-gas studies may reveal small chain motions induced by CO_2 sorption that can facilitate the diffusion of the larger CH_4 gas without affecting the transport of the smaller CO_2 in a pure-gas study. In previous work, we demonstrated that these "second-component effects" can even occur for carbon membranes (600−800 °C) derived from pyrolysis of a PIM-PI precursor PIM-6FDA-OH.[22,35]

To date, there are no studies detailing the mixed-gas CO_2/CH_4 transport properties of the recently reported, highly rigid bridged-bicyclic-based PIMs and PIM-PIs. This paper investigates two PIM-PIs based on the fused-ring and intramolecularly rigid 9,10-diisopropyltriptycene dianhydride (TPDA). One contains an ortho-substituted and rotation-restricted *N*-phenyl−imide bond—KAUST-PI-1 (TPDA-TMPD)—and the other has a relatively flexible diamine and *N*-phenyl−imide bond—KAUST-PI-5 (TPDA-6FpDA).[46,47] Results of physical microstructural investigations are analyzed

dx.doi.org/10.1021/ma501798v | *Macromolecules* XXXX, XXX, XXX−XXX

together with those of high-pressure pure- and mixed-gas CO_2/CH_4 transport properties for thick films of the polyimides and the commercial standard, cellulose acetate, for reference. The objective is to provide representative comparisons that address, on a physical basis, whether the intrachain rigidity central to the design of PIMs for highly permeable and selective O_2 and H_2 separations can support intrinsic plasticization resistance in the presence of aggressive CO_2-based mixtures.

2. EXPERIMENTAL SECTION

2.1. Polymer Synthesis. KAUST-PI-1 (TPDA-TMPD) and KAUST-PI-5 (TPDA-6FpDA) were synthesized by the reaction of the previously reported 9,10-diisopropyl dianhydride (TPDA) with tetramethylphenylenediamine (TMPD) and 4,4′-(hexafluoroisopropylidene)dianiline (6FpDA), respectively (Figure 1). Full synthetic details and characterizations for all monomers and the polymers are available elsewhere.[46,47] The polymer synthesis is summarized here. A solution of the diamine (1.0 mmol) and freshly distilled *m*-cresol (7 mL) was stirred for 5 min in a 25 mL reaction tube under nitrogen flow. To this mixture, 1.0 mmol of the TPDA dianhydride monomer and 0.1 mL of isoquinoline were added. After stirring for 1 h, the temperature was raised to 200 °C and held for 4 h. Water formed by the imidization reaction was removed by azeotropic distillation using anhydrous toluene. After cooling to room temperature (22 °C), the polyimide was obtained by dropwise addition of the polymer solution to methanol. The solid was filtered, purified by reprecipitation from chloroform into methanol, and then dried at 120 °C in a vacuum oven for 24 h. Cellulose triacetate (acetyl content = 43.6%, degree of substitution (DS) ∼ 2.9) was obtained as pellets from Eastman (CA-436-80S).

2.2. Structural and Physical Properties. *2.2.1. Molecular Simulation.* The polyimide repeat units were constructed in Materials Studio (Accelrys, 7.0), and relevant dihedral angles (e.g., across the *N*-phenyl−imide bonds) were identified as indicated in Figure 1. The Conformer module was used to incrementally vary the dihedral angle between −180° and +180° while energy minimizations of each conformer were performed with the Forcite module (COMPASS force field, Smart algorithm). The energy barriers to changes in the dihedral angles were calculated relative to the lowest energy attained ($\Delta E = E_i - E_{min}$) over the 360° range. As a first approximation of the degrees of torsional freedom available at the transport testing temperature (35 °C), the available thermal energy was estimated as 3*RT*.

2.2.2. Low-Pressure Physisorption and Pore-Size Distribution Analysis. Nitrogen (−196 °C) and carbon dioxide (0 °C) sorption measurements were performed up to 1 bar using a Micromeritics ASAP 2020 apparatus with a micropore upgrade. Powder samples of the polyimides were dried under high vacuum at 120 °C for 15 h before measurement. Free space measurements were done with helium. The data were collected and analyzed using ASAP 2020 software version 4.02. Equilibrium values were determined when <0.01% change occurred in the average pressure measured at intervals of 10 s. Typically, an experiment with N_2 required 48 h, whereas that with CO_2 required less than 24 h. Shifts in the pore-size distributions of the polyimides caused by the change in diamine were qualitatively evaluated using NLDFT (non-local density functional theory) analysis of the N_2 and CO_2 isotherms. Although this model was originally developed for carbons, it has been increasingly advocated for amorphous polymers[55−57] partly because the smaller and more condensable CO_2 molecule can access narrower porosity at temperatures closer to those used in permeation testing (35 °C). The physical state of the soft polymer matrix is thus comparable.[56] In these experiments, the temperature is set at 0 °C due to NLDFT model availability. Moreover, our previously reported data for PIM-1 and poly(1-trimethylsilyl-1-propyne) (PTMSP) powders are included for comparison.[46]

2.2.3. High-Pressure Equilibrium Sorption. High-pressure CO_2 and CH_4 sorption isotherms were collected gravimetrically up to 20 bar on powder samples of the PIM-PIs at 35 °C using a Hiden IGA system (UK) with a microbalance. All samples were degassed for at least 24 h under high vacuum prior to the collection of each isotherm. The solubility coefficients, *S* (cm^3 (STP) cm^{-3} $cmHg^{-1}$), were calculated at each pressure from the gas concentration, *c* (cm^3 (STP) cm^{-3}), and the pressure, *p* (cmHg), by

$$S = \frac{c}{p} \tag{1}$$

The solubility selectivity is then given by a ratio of component solubilities. Each pressure point was held until minimal changes (<2%) were observed in sorption/time uptake plots (typically <24 h). Additionally, CH_4 sorption isotherms were collected prior to CO_2 exposure.

2.3. Polymer Film Preparation. Dense polymer films were obtained by slow evaporation of filtered 3−5 wt % polymer solutions cast on a leveled glass plate. The PIM-PIs were cast from chloroform and CA from dichloromethane. The resulting membranes were first dried at 120 °C for 24 h in a vacuum oven, soaked in methanol at room temperature for 24 h, and finally dried at 120 °C for 24 h under high vacuum to remove any residual casting solvent trapped in the micropores during casting. Thermal gravimetric analysis (TGA) confirmed solvent removal. The effective areas and thicknesses (∼70 μm) of the films were determined by calibrated scanning software and a digital micrometer, respectively.

2.4. Pure- and Mixed-Gas Permeation. *2.4.1. Pure-Gas Permeation.* The pure-gas permeabilities of the dense films were determined using the constant-volume/variable-pressure method. The membranes were degassed in the permeation test apparatus on both sides under high vacuum at 35 °C. For the polyimides, regular measurements of O_2 and N_2 permeabilities were performed until they varied negligibly with time (after ∼15 days), indicating relaxation of the excess free volume induced by methanol conditioning. CA dense films did not exhibit time-dependent permeation properties on the experimental time scale. The increase in permeate pressure with time was measured by a 100 Torr MKS Baratron transducer. The CO_2 and CH_4 pure-gas permeabilities were measured at 35 °C at 2, 5, 10, and 15 bar and calculated by

$$P = \mathrm{DS} = 10^{10}\frac{V_d l}{p_{up} A R T}\frac{dp}{dt} \tag{2}$$

where *P* is the gas permeability (in barrer) (1 barrer = 10^{-10} cm^3 (STP) cm cm^{-2} s^{-1} $cmHg^{-1}$), p_{up} is the upstream pressure (cmHg), dp/dt is the steady-state permeate side pressure increase (cmHg s^{-1}), V_d is the calibrated permeate volume (cm^3), *l* is the membrane thickness (cm), *A* is the effective membrane area (cm^2), *T* is the operating temperature (K), and *R* is the gas constant (0.278 cm^3 cmHg cm^{-3} (STP) K^{-1}). The ideal permselectivity ($\alpha_{A/B}$) for separation of A/B was calculated by

$$\alpha_B^A = \frac{P_A}{P_B} \tag{3}$$

For each polymer, permeation data are presented as an average of duplicate measurements performed on two separate films.

2.4.2. Mixed-Gas Permeation Measurements. The mixed-gas permeation properties for the dense films were measured at 35 °C with a 50:50 CO_2/CH_4 binary mixture using a setup similar to that previously described by O'Brien et al.[58] The films were tested at total pressures of 4, 10, 20, and 30 bar such that the mixed-gas CO_2 partial pressures were equal to those used in the pure CO_2 permeation experiments. This methodology permits direct comparison of the pure- and mixed-gas data to elucidate any nonidealities including plasticization and competitive sorption. The stage cut, that is, the ratio of permeate to feed flow rates, was less than 0.01 to ensure that the residue composition was essentially equal to that of the feed gas. CO_2 and CH_4 concentrations were measured with a calibrated gas chromatograph (Agilent 3000A Micro GC) equipped with thermal conductivity detectors. The mixed-gas permeability of component *i* was determined by

dx.doi.org/10.1021/ma501798v | Macromolecules XXXX, XXX, XXX−XXX

$$P_i = 10^{10}\frac{y_i V_d l}{x_i p_{up,i} ART}\frac{dp}{dt} \quad (4)$$

where y and x are the mole fractions in the permeate and feed, respectively, and $p_{up,i}$ is the upstream partial pressure of component i. Because the downstream pressure was negligible, the mixed-gas selectivity of component i/j was obtained from

$$\alpha_{i/j} = \frac{y_i/y_j}{x_i/x_j} \quad (5)$$

Steady-state permeation was identified at each feed pressure when regular measurements of permeability and selectivity *both* changed negligibly with time. For each polymer, permeation data are presented as an average of duplicate measurements performed on two separate films.

3. RESULTS AND DISCUSSION

3.1. Physical and Structural Properties. *3.1.1. Polymers and Simulated intrachain Flexibilities.* KAUST-PI-1 and KAUST-PI-5 were synthesized in high molecular weight as determined by gel permeation chromatography (Malvern HT-350) with polystyrene as an external standard (Table 1). No T_g was observed from −80 to 350 °C in differential scanning calorimetry measurements for either polymer, even shortly after exposure to 20 bar of CO_2 for 72 h. This probably reflects limitations on large macromolecular motions (i.e., necessary to enter a rubbery state) in glassy PIM-PIs based on the fused-ring triptycene-containing dianhydride TPDA.

Table 1. Physical Properties of KAUST-PI-1 and KAUST-PI-5

polymer	M_w (g mol^{-1})	M_w/M_n	BET surface area (m^2 g^{-1})	T_g (°C)	ρ^b (g cm^{-3})
KAUST-PI-1	158000	2.0	750	>350	1.09
KAUST-PI-5	83000	2.0	500[a]	>350	1.34

[a]Calculated from isotherms measured in this work on a Micromeritics ASAP 2020 apparatus equipped with a "micropore option". [b]Film density was determined by measurement of buoyancy with helium (Hiden, IGA).

Since rigidity is central to the discussions in this work, an important subtlety is emphasized and illustrated in Figure 2. Briefly, polymer "rigidity" can be intrachain or interchain in nature. For example, intrachain rigidity can result from restricted backbone torsions within a chain. On the other hand, high interchain rigidity can result from physical interactions or covalent bonds between chains that may restrict macromolecular motion and limit dilation.

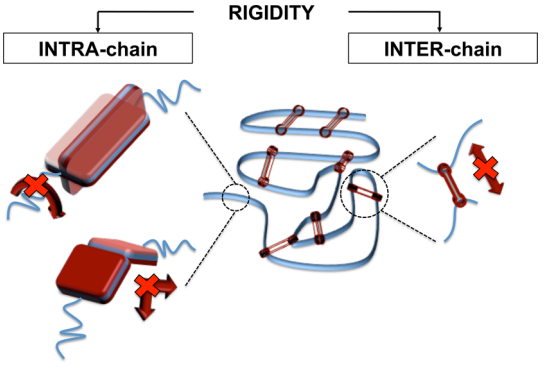

Figure 2. Classification of polymer "rigidity" into intrachain and interchain rigidity. The blue ribbon in the illustration represents a polymer chain.

Figure 3 demonstrates some characteristic dihedral angle distributions about bonds highlighted in Figure 1. This analysis is a first approximation of the differences in intrachain rigidity between the two polyimides because repeat units, and not densely packed chains, were used in the simulations. KAUST-PI-1 shows significantly higher intrachain rigidity than KAUST-PI-5 due to steric interference between the methyl groups of the TMPD diamine and the carbonyl groups of the imide ring, restricting rotation about the *N*-phenyl−imide bond. The 6FpDA diamine in KAUST-PI-5 adds considerable intrachain flexibility at two locations in the backbone: (i) the *N*-phenyl−imide bond, which is not substituted, and (ii) at the bonds between the phenyl rings. This flexibility in 6FpDA facilitates coplanarization of the backbones and improves chain stacking. It is a key reason behind the success of 6FpDA in improving the plasticization resistances of promising polyimides[29] and polyamide−imides.[30,32] Indeed, fluorescence excitation spectra are red-shifted for a thick film of KAUST-PI-5 relative to KAUST-PI-1, probably due to the formation of intermolecular charge transfer complexes in the flexible and more densely packed KAUST-PI-5 (Figure S1, Supporting Information).[59,60] This is consistent with results for 6FDA-DAM (rigid *N*-phenyl bond) and 6FDA-6FpDA (flexible *N*-phenyl bond) reported by Vaughn and Koros.[32] Accordingly, this bodes well for the plasticization resistance of the more flexible KAUST-PI-5.

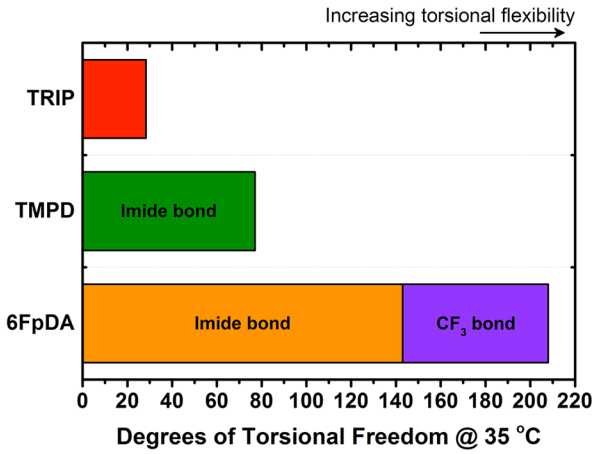

Figure 3. Distributions in the dihedral angles highlighted in the repeat unit structures of Figure 1 (Conformers module, Materials Studio 7.0, Accelrys). "TRIP" refers to the triptycene contortion site in the dianhydride monomer. TMPD and 6FpDA are the diamines in KAUST-PI-1 and KAUST-PI-5, respectively.

3.1.2. Low-Pressure Physisorption and Pore-Size Distributions. Low-pressure physisorption is a useful technique for qualitatively exploring the effects of the diamine (TMPD, 6FpdA) on the amount and distribution of porosity in the PIM-PI microstructures.[55−57,61,62] The conclusions in this section provide the physical basis for later discussion of pure- and mixed-gas transport properties. Sorption isotherms of N_2 (−196 °C) and CO_2 (0 °C) are shown in Figure 4 for KAUST-PI-1 and KAUST-PI-5 in comparison to microporous PIM-1 and PTMSP. All isotherms are similarly shaped and indicative of microporous materials (IUPAC, pore diameter <20 Å) possessing interconnected porosity. KAUST-PI-1

dx.doi.org/10.1021/ma501798v | Macromolecules XXXX, XXX, XXX−XXX

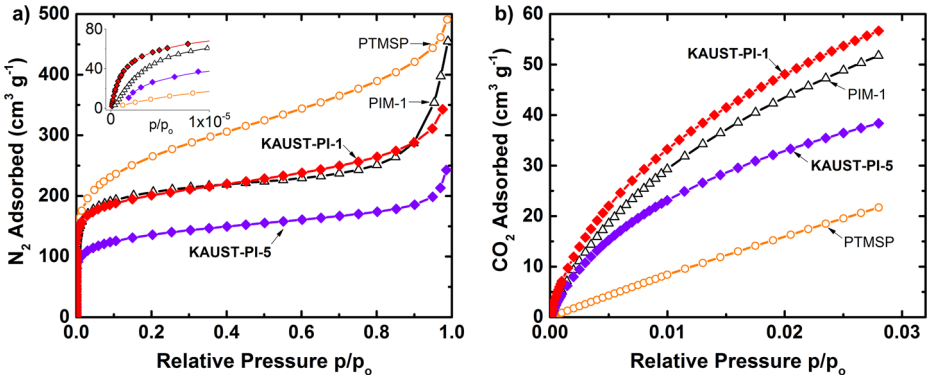

Figure 4. Sorption isotherms for (a) N_2 (−196 °C, p_0 = 1 bar) and (b) CO_2 (0 °C, p_0 = 33 bar) collected up to 1 bar for KAUST-PI-1, KAUST-PI-5, PIM-1, and PTMSP.

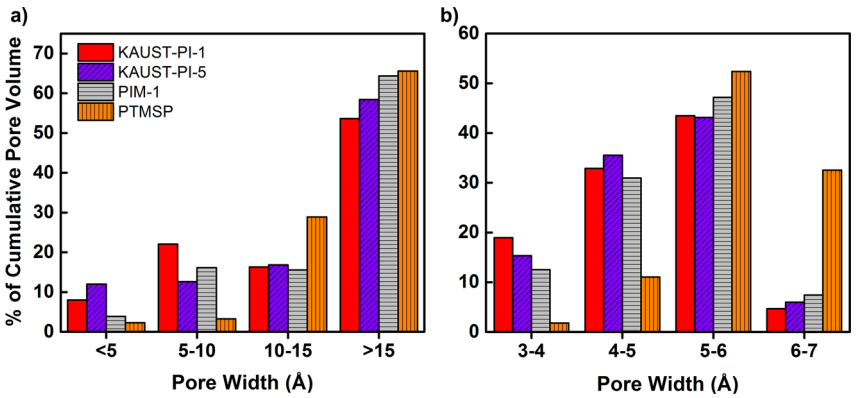

Figure 5. Pore-size distributions (PSDs) represented as the distribution of cumulative pore volume against pore width. PSDs were derived from NLDFT analysis of (a) N_2 and (b) CO_2 sorption isotherms in Figure 4 assuming carbon slit pores.

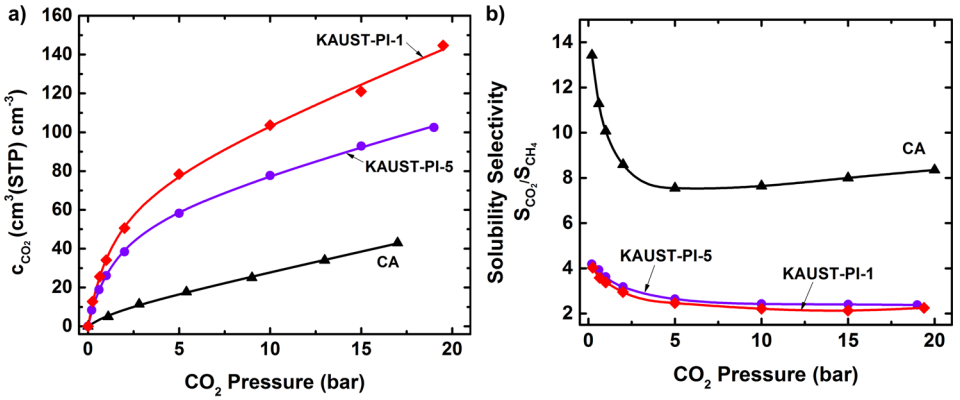

Figure 6. High-pressure (a) equilibrium CO_2 sorption isotherms for KAUST-PI-1, KAUST-PI-5, and CA and (b) the corresponding pure-gas solubility selectivities. The data for CA (DS = 2.84) were taken from Puleo et al.[37]

demonstrates roughly 2-fold higher N_2 and CO_2 uptakes than KAUST-PI-5 particularly in the low-pressure ranges where adsorption preferentially occurs in micropores. A higher BET surface area was also calculated for KAUST-PI-1 (750 m^2 g^{-1}) relative to KAUST-PI-5 (500 m^2 g^{-1}). Concisely, the greater microporosity evident in KAUST-PI-1 is attributed to the higher intrachain rigidity imparted by the short and bulky TMPD diamine, which is known to disrupt chain packing and trap microporosity.[63−65] On the other hand, KAUST-PI-5 (ρ = 1.34 g cm^{-3}) packs more densely than KAUST-PI-1 (ρ = 1.09 g cm^{-3}) owing to the intrachain flexibility in the 6FpDA diamine (Figure 3).

NLDFT-based pore-size distributions (PSDs) were calculated from the N_2 and CO_2 isotherms of Figure 4 and shown in Figure 5 as distributions in cumulative pore volume over pore width. Two important features appear. First, KAUST-PI-1 has a larger *fraction* of narrower micropores than KAUST-PI-5, PIM-1, and PTMSP. This is consistent with its higher diffusion selectivities due to greater molecular sieving properties.[46,47] Importantly, it indicates a higher degree of "order" in the microstructure of KAUST-PI-1 that should be more susceptible to small dilations caused, for example, by CO_2-induced plasticization. Second, both polyimides appear to have similar *fractions* of larger pores; however, the *amount* of either (large and small pores) is greater in KAUST-PI-1 than KAUST-PI-5

dx.doi.org/10.1021/ma501798v | *Macromolecules* XXXX, XXX, XXX−XXX

given its larger surface area (Table 1). Relative to microporous PIM-1 (770 m^2 g^{-1}, 0.66 cm^3 g^{-1}) and PTMSP (950 m^2 g^{-1}, 0.71 cm^3 g^{-1}), KAUST-PI-1 shows (i) lower pore volume, (ii) larger fractions of small pores, and (iii) smaller fractions of large pores. PIM-1 and PTMSP form "reverse-selective" membranes with the highest *n*-C_4H_{10}/CH_4 mixed-gas selectivities and *n*-C_4H_{10} permeabilities exceeding those of smaller molecules.[66,67] This is consistent with the greater presence of larger free-volume elements accessible enough to accommodate the *n*-C_4H_{10} vapor.

3.1.3. High-Pressure Equilibrium Sorption. There have been several notable attempts to correlate a critical amount of CO_2 (e.g., concentration, partial molar volume) sorbed in a polyimide matrix with the occurrence of a "plasticization pressure" at which an upturn appears in the pure-gas CO_2 permeability isotherm.[7,8,68] Figure 6a shows that the CO_2 concentration in the PIM-PIs was at least 3 times greater than in CA. At ~2 bar partial pressure (vs 10 bar for CA), both PIM-PIs surpassed the critical CO_2 concentration of 36 ± 7 cm^3 (STP) cm^{-3} polymer proposed by Bos et al.[68] to trigger a "plasticization pressure". Additionally, KAUST-PI-1 sorbed ~50% more CO_2 and CH_4 (Figure S2) than KAUST-PI-5 across the 20 bar pressure range. This is related to its more microporous structure as discussed above in section 3.1.2 and evidenced by higher C_H' and k_D parameters calculated from dual-mode model fits to the concentration isotherms (Table S1). Based on these observations, early plasticization is expected for both polyimides.

Despite the disparity in sorption capacities of the PIM-PIs, there were negligible differences between their CO_2/CH_4 solubility selectivities (Figure 6b). They were only slightly lower for KAUST-PI-1 probably due to easier access of the CH_4 molecule into its more open porosity, as recently noted for PIM-type materials.[69] Moreover, the solubility selectivities of both PIM-PIs (ranging from 2 to 4 across the 20 bar pressure range) are comparable to those of conventional low-free-volume polyimides (ranging from 3 to 4).[70] CA has been shown to exhibit anomalously high solubility selectivities up to 4 times those of polyimides, but without speculating on the reasons for this behavior, we found that only weak physisorption (heat of adsorption ~25−30 kJ mol^{-1}) occurs in both CA and KAUST-PI-1 (Figure S9). It thus seems that the sorption and, subsequently, permeation behaviors in polymers are dominated by physical factors (e.g., amount and distribution in porosity) and not any special interactions with CO_2.

3.2. Pure- and Mixed-Gas Permeation. *3.2.1. Aging Knee.* Before measurement of all permeation data, the freshly methanol-conditioned and heat-dried (120 °C) PIM-PI films were kept under vacuum in the permeation testing apparatus as their O_2/N_2 transport properties were monitored with time. Two general stages of time-dependent permeation were observed: (i) ~10−15 days of rapid permeability loss and selectivity increase consistent with a relaxation of the excess free volume induced by methanol conditioning and (ii) ~15−150 days that demonstrated negligible time dependence on the experimental time scale. The trends have been shown to be diffusion-dominated, supporting some physical rearrangement and densification of the microstructure.[47] Moreover, we recently proposed measuring gas transport properties of PIMs at the onset of the second stage—so-called "aging knee"[47]—to promote reproducibility and consistency of their dense-film data across the literature. That is, the kinetics in thin films (~200 nm) can be very different.[71] Figure 7 demonstrates similar relaxation behaviors of methanol-conditioned KAUST-PI-1 and KAUST-PI-5 with time, which resemble that of microporous PIM-1.[72] Therefore, all data reported in this work were taken at (and shortly after) the aging knee highlighted in Figure 7.

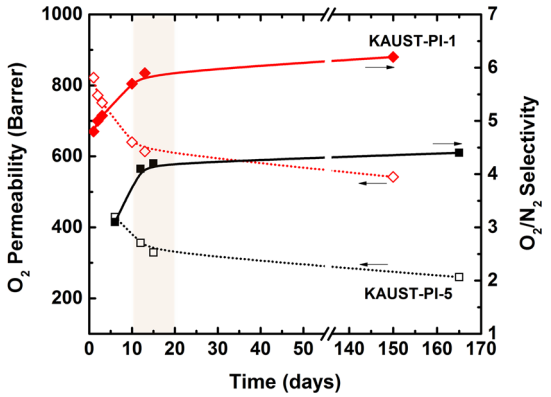

Figure 7. Identification of an "aging knee" (highlighted region, 10−15 days) where the time dependence of gas transport properties in methanol-conditioned KAUST-PI-1 and KAUST-PI-5 reached a quasi-steady state. This provides for more consistent and reproducible data.

3.2.2. CO_2/CH_4 Separation. The pressure dependence of the pure- and mixed-gas permeability isotherms for dense films (~70 μm) of KAUST-PI-1, KAUST-PI-5, and CA is shown in Figure 8a,b. Unexpectedly, KAUST-PI-1 underwent significant plasticization evidenced by immediate rises in its pure- and mixed-gas CO_2 permeabilities with pressure. This behavior is reminiscent of thin-film mixed-gas behavior (e.g., CA), which is unusual given that thin films typically exhibit more extensive and accelerated plasticization responses than thick films.[73] Sanders et al. proposed that this cannot be explained purely by sorption capacity.[15] Indeed, although PIM-1[74] and KAUST-PI-1 sorb nearly the same amount of CO_2 (140 cm^3 g^{-1} at 20 bar of CO_2), their permeation behaviors are different in that (i) mixed-gas CO_2 permeability exhibits a dual-mode-type decrease with pressure in PIM-1 but immediate pressure-dependent increases in KAUST-PI-1 and (ii) the extent of mixed-gas CH_4 permeability increase (an unambiguous indication of plasticization) is 5 times more in KAUST-PI-1 (~300%) than in PIM-1 (60%) at comparable CO_2 partial pressures (10−15 bar).[34]

On the other hand, the more flexible (Figure 3) KAUST-PI-5 is considerably more plasticization resistant than KAUST-PI-1 (Figure 8). The permeability isotherms initially decreased with pressure as the Langmuir sites saturated, consistent with the dual-mode model. A slight upturn in the pure-gas CO_2 permeability isotherm then appeared at 10 bar of CO_2 partial pressure (Figure 8a), as for CA. It does not correspond to the critical CO_2 concentration suggested by Bos et al.,[68] which occurred at 2 bar (Figure 6a). In fact, KAUST-PI-5 required 4 times more CO_2 than CA to achieve a similar plasticization response (i.e., at the same CO_2 partial pressure of 10 bar). Although it did not sorb much less than KAUST-PI-1, the pure-gas D_{CO_2} in KAUST-PI-1 increased 2 times more with CO_2 pressure (concentration) than in KAUST-PI-5 for an absolute 4-fold increase between 2 and 20 bar (Figure S6). The permeation trends are therefore diffusion-dominated and again (as discussed for KAUST-PI-1 above) not purely related to

dx.doi.org/10.1021/ma501798v | *Macromolecules* XXXX, XXX, XXX−XXX

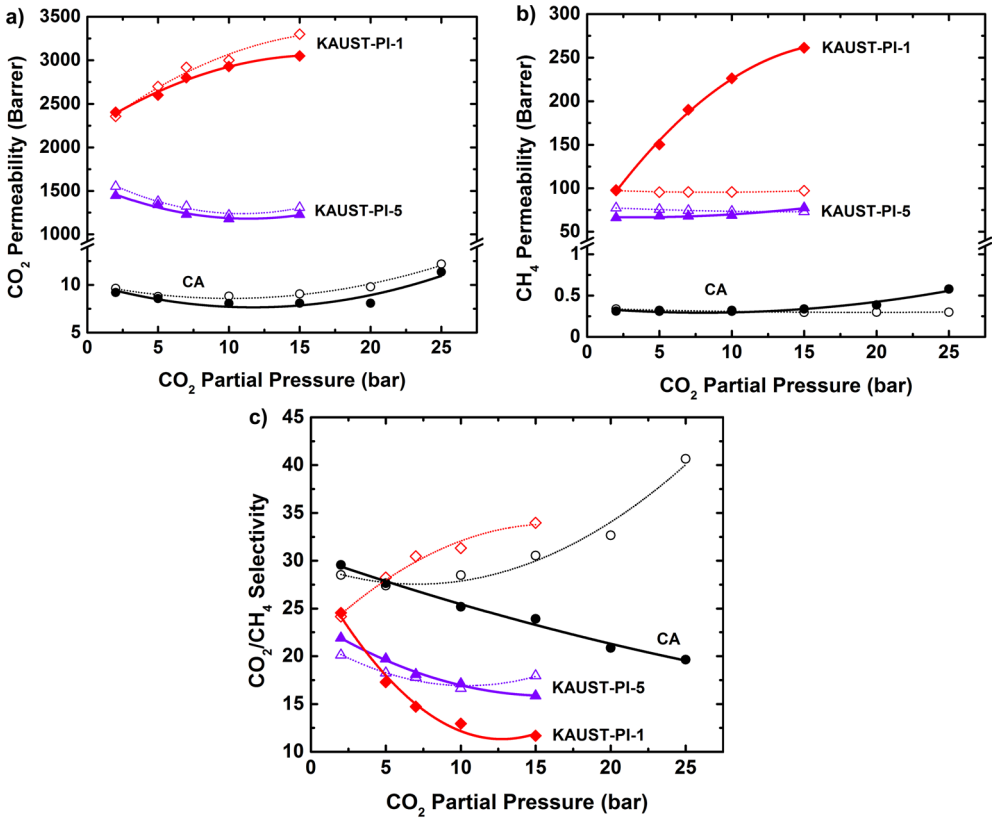

Figure 8. Pressure dependence of pure- and mixed-gas (a) CO_2 and (b) CH_4 permeability isotherms and (c) CO_2/CH_4 selectivity (T = 35 °C, 50:50 CO_2:CH_4 mixture) for KAUST-PI-1, KAUST-PI-5, and CA (DS ∼ 2.9). Open points: pure-gas feed. Closed points: mixed-gas feed.

sorption capacity. Moreover, the CH_4 permeability (Figure 8b) was relatively flat in the mixed-gas and close to that in the pure-gas experiments. It increased slightly around 10 bar CO_2 partial pressure, in agreement with the upturn in the pure-gas CO_2 isotherm and reflects enhanced CH_4 diffusion as a result of slight CO_2-induced microstructural dilations. This behavior is qualitatively similar to that seen for CA. Competitive sorption slightly reduces CO_2 permeabilities in the mixed gas relative to the pure gas for all polymers, but the effect is small relative to that of plasticization.

Accordingly, two intriguing points emerge for discussion considering the above observations and the high intrachain rigidity of KAUST-PI-1: (i) Why is the effect/extent of CO_2-induced plasticization greater in KAUST-PI-1 than in KAUST-PI-5, PIM-1, and CA (all thick films)? (ii) Why is plasticization accelerated in KAUST-PI-1 (i.e., immediate rises in pure- and mixed-gas CO_2 permeability isotherms and mixed-gas CH_4 permeability isotherm from 2 bar)? Both questions may be answered on a physical basis inspired by the microstructural investigation in section 3.1.2. Regarding the first question, we hypothesize that the more extensive plasticization of KAUST-PI-1 can be traced to the higher "order" of its microstructure—i.e., the larger presence of tighter molecular sieving pores.[75] That is, Figure 5 shows a higher proportion of smaller ultramicropores in KAUST-PI-1 than in PIM-1 and KAUST-PI-5. Given the combination of high O_2 permeability (∼600 barrers) with high O_2/N_2 selectivities (∼6.0) in KAUST-PI-1,[46,47] these pores contribute significantly to transport and likely comprise a considerable fraction dimensioned around O_2 and N_2 at 3−4 Å. Their dilation would influence the transport of CO_2 because its molecular diameter is also in that range, between that of O_2 and N_2 as indicated by the ranking of diffusion coefficients ($D_{N_2} < D_{CO_2} < D_{O_2}$). This is consistent with the rises in CO_2 permeability isotherms in KAUST-PI-1 and supported by an additional experimental observation: 2-fold increase in N_2 permeability concurrent with a drop in O_2/N_2 selectivity to 3−4, as measured after the 30 bar mixed-gas point (plasticized microstructure). For similar reasons, the bigger CH_4 (k_D = 3.8 Å) gas is usually affected to a greater extent than CO_2 (Figure 8b). Furthermore, although dilations also occur in PIM-1 as indicated by the 60% increase in mixed-gas CH_4 permeabilities over pure-gas values, its CO_2 permeability decreases with pressure (in sharp contrast to the rise in that of KAUST-PI-1). As far as the pure-gas permeability isotherm indicates, the smaller CO_2 molecule is relatively unaffected in PIM-1 given the larger contribution (and presence) of bigger, easily accessible pores to its transport properties. This physical difference is the basis for a nearly 2-fold higher CO_2 diffusion coefficient in PIM-1 (83×10^{-8} cm^2 s^{-1}) at 2 bar than in KAUST-PI-1 (46×10^{-8} cm^2 s^{-1}) as well as generally 3-fold higher gas permeabilities in PIM-1.[34,46] Interestingly, the *distribution* of porosity in KAUST-PI-5 is similar to that in PIM-1 in that it lacks the narrow ultramicroporosity characteristic of KAUST-PI-1 (Figure 5). We therefore believe that the greater effect of plasticization on KAUST-PI-1 (i.e., sharp rises in CO_2 and CH_4 permeability isotherms) relative to KAUST-PI-5 is based on these fundamental *physical* differences, whereby its more highly sieving ultramicroporosity is more sensitive to CO_2-induced dilations.

The second question is posed regarding the "earlier," accelerated plasticization of KAUST-PI-1 despite its high

dx.doi.org/10.1021/ma501798v | *Macromolecules* XXXX, XXX, XXX−XXX

intrachain rigidity. Previously, it was concluded that a structural change to a conventional low-free-volume polyimide could simultaneously boost permeability and selectivity if gains and losses in intrachain *mobility* and interchain *packing* were balanced.[76] It was observed, moreover, that the most significant improvements were achieved when both were inhibited. As a slight modification to that conclusion, we hypothesize that a structural change to a PIM-type polyimide could increase intrinsic plasticization resistance in mixed-gas CO_2/CH_4 feeds if gains and losses in interchain *spacing* and interchain *interactions* are balanced. Increasing interchain interactions is emphasized. This can be facilitated by bringing chains closer together (reducing interchain spacing) and coplanarizing the polyimide backbone, both of which can be promoted by an increased intrachain mobility (Figure 2) as previous work has shown.[32] Here, the balance is discussed in terms of substituting the 6FpDA diamine (KAUST-PI-5) with TMPD (KAUST-PI-1). The bulky CF_3 groups of 6FpDA increase interchain spacing, which reduces the prospect of interchain interaction. However, the intrinsic flexibility of the 6FpDA diamine (Figure 3) appears to dominate in promoting denser chain packing, backbone coplanarization, and consequently better interchain interactions (e.g., CTCs). This was suggested by the red-shift in its fluorescence excitation spectra relative to KAUST-PI-1 (Figure S1). Such interchain interactions can mitigate the chain mobility that ultimately loosens the microstructure and facilitates diffusion in plasticization. With TMPD, the four methyl groups serve to increase interchain spacing in two ways: (i) by virtue of their bulkiness and (ii) by "locking" up the *N*-phenyl−imide bond, preventing the local segmental motions necessary for denser packing. Accordingly, interchain interactions are compromised in two interdependent ways: (i) large free volume increases throughout the microstructure relative to KAUST-PI-5 (e.g., 50% increase in BET surface area, ∼2−3-fold increase in CO_2 permeability) and (ii) restriction on the ability of the diamine to coplanarize with the dianhydride. Briefly, KAUST-PI-1 is more susceptible to matrix dilation because its highly disrupted packing compromises interchain rigidity.

Previous work offers several hints that these observations regarding the consequences of intrachain rigidity have a broader applicability to other classes of polymeric materials. For example, restriction of backbone flexibility in a bisphenol A polycarbonate via tetramethyl substitution (increasing T_g[77] from 150 to 200 °C) results in far earlier plasticization (a decrease in its pure-gas plasticization pressure from 31 to 13 bar).[68] Additionally, if the TPDA dianhydride in KAUST-PI-1 is replaced with a more flexible 6FDA dianhydride (i.e., 6FDA-durene), a typical dual-mode type CO_2 permeability isotherm appears with a clear upturn at 10 bar of CO_2.[28] Relative to KAUST-PI-1, this represents greatly improved plasticization resistance. Similarly, CA also demonstrates higher plasticization resistance than KAUST-PI-1 in pure- and mixed-gas experiments (Figure 8) although it has a flexible backbone comprising ether-linked rings. The presence of interchain acetyl−acetyl and acetyl−hydroxyl interactions in CA (strengthened in a relatively dense packing promoted by looser chain backbones) contribute interchain rigidity. Ultimately, this work demonstrates that the intrachain rigidity central to PIM design principles is not a singular solution to intrinsic plasticization suppression in PIM-type polyimides. Instead, it appears that a departure from this design principle is required and will be reported on in another publication.

Finally, indirect evidence of chain motion in KAUST-PI-1 is clear in the time dependence of the permeation properties during CO_2-induced plasticization. Figure 9 provides a

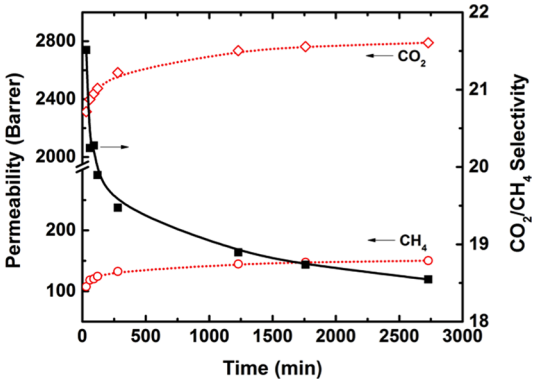

Figure 9. Time dependence in KAUST-PI-1 of mixed-gas CO_2/CH_4 permeation properties at 20 bar total pressure (50:50 CO_2:CH_4, 35 °C). Microstructural reorganization kinetics during CO_2-induced plasticization are indicated.

representative example of the reorganizational kinetics of the KAUST-PI-1 matrix during CO_2-induced plasticization in the 20 bar mixed-gas experiment (10 bar CO_2 partial pressure). Both CO_2 and CH_4 permeabilities increase and CO_2/CH_4 selectivity decreases until stabilizing at ∼3000 min. Chain motions are occurring, albeit relatively slowly given that the diffusion time lag of CO_2 at 2 bar is less than 30 s. This reflects the fact that intrasegmental rotations are sterically hindered in KAUST-PI-1.

3.2.3. Permeability/Selectivity Trade-Off Map. For reference, the permeability/selectivity trade-off map for pure- and mixed-gas CO_2/CH_4 separations is shown with the latest upper bound[52,67] in Figure 10. Because the upper bound is derived

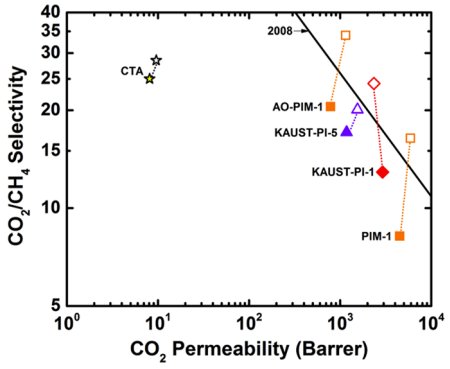

Figure 10. Permeability/selectivity trade-off map for CO_2/CH_4 separation. Conditions for CO_2/CH_4 data: T = 35 °C; open points, 2 bar, pure-gas feeds; closed points, 20 bar, 50:50 CO_2/CH_4 feed. Solid line is the latest 2008 upper bound.

from pure-gas data, it cannot suitably gauge the performance of polymers in CO_2/CH_4 separation. Figure 10 illustrates the large changes in permeabilities and, particularly, selectivities that can occur between pure-gas data (open points) and mixed-gas data (closed points) due to nonideal effects (e.g., competitive sorption, plasticization). The advances in PIM-type materials for the CO_2/CH_4 separation generally remain permeability-driven toward the lower right corner of Figure 10, although selectivity is paramount to the economic viability of a

dx.doi.org/10.1021/ma501798v | *Macromolecules* XXXX, XXX, XXX−XXX

membrane process under the high-pressure ratios involved in CO_2/CH_4 separations. Therefore, research efforts need to be directed toward increasing selectivity in sour mixed-gas feeds to at least that offered by the commercial standard, CA. The goal of this work was to offer guidance toward that end.

4. CONCLUSIONS

High-pressure pure- and mixed-gas CO_2/CH_4 permeation and sorption-based microstructural characterizations were conducted for two ultramicroporous PIM-type polyimides. They were analyzed for general structure−property relationships that can guide the rational design of a polymer intrinsically resistant to CO_2-induced plasticization in mixed-gas feeds. Specifically, the role of intrachain rigidity—central to the design of rapidly emerging PIMs—was investigated in a comparison of KAUST-PI-1—possessing a highly rotation-restricted backbone comprising a fused-ring bridged-bicyclic-based dianhydride (TPDA) and rotation-restricted *N*-phenyl−imide bond—with KAUST-PI-5, in which the TMPD diamine of KAUST-PI-1 was substituted with the more flexible 6FpDA diamine. Preliminary conclusions obtained in the context of pure- and mixed-gas CO_2 separation appear to favor a departure from the torsion-resistant backbones normally targeted in "conventional PIMs" for high permeability and high selectivity in O_2 and H_2 separations. Specifically:

a. The intrachain rigidity central to PIM design is not a singular solution to intrinsic plasticization mitigation. Instead, a balance between interchain rigidity (e.g., via dipole−dipole interactions, hydrogen-bonding, charge-transfer complexes) and interchain spacing is emphasized in the design and composition of the repeat unit.

b. The amount and distribution of interconnected microporosity in PIMs are critical, as opposed to purely sorption capacity. A more highly sieving microstructure in which narrower ultramicropores (e.g., KAUST-PI-1) contribute significantly to transport is notably more sensitive to plasticization. Such a microstructure is promoted by intrachain rigidity and suggests that these design considerations need to be made in the development of highly selective and intrinsically plasticization resistant PIMs.

c. Unexpectedly, some intrachain flexibility permitting local segmental motion seems to mitigate such plasticization. That is, relatively flexible backbones (e.g., KAUST-PI-5) are more likely to coplanarize, assume a denser packing configuration and engage in interchain interactions that restrict chain mobility and plasticization.

d. Solubility selectivities ranged from 3 to 4 for the PIM-PIs, comparable to those in conventional low-free-volume polyimides. Additionally, only weak physisorption was observed for CO_2 in KAUST-PI-1 and CA as evidenced by heats of adsorption (~30 kJ mol^{-1}). Plasticization was thus observed to be diffusion-dominated, as the pure-gas-based D_{CO_2} rose with pressure faster than S_{CO_2} dropped with pressure.

■ ASSOCIATED CONTENT

Supporting Information

Fluorescence excitation spectra, pressure dependence of diffusivity and solubility coefficients for CO_2 and CH_4 in PIM-PIs and CA, isosteric heats of adsorption, additional sorption isotherms for CO_2 and CH_4. This material is available free of charge via the Internet at http://pubs.acs.org.

■ AUTHOR INFORMATION

Corresponding Author

*E-mail: Ingo.Pinnau@kaust.edu.sa (I.P.).

Notes

The authors declare no competing financial interest.

■ ACKNOWLEDGMENTS

The authors acknowledge financial support of this work by KAUST funding for Prof. Ingo Pinnau.

■ REFERENCES

(1) Baker, R. W.; Lokhandwala, K. *Ind. Eng. Chem. Res.* **2008**, *47*, 2109−2121.
(2) Baker, R. W. *Ind. Eng. Chem. Res.* **2002**, *41*, 1393−1411.
(3) Bhide, B. D.; Stern, S. A. *J. Membr. Sci.* **1993**, *81*, 239−252.
(4) Hachisuka, H.; Sato, T.; Imai, T.; Tsujita, Y.; Takizawa, A.; Kinoshita, T. *Polym. J.* **1990**, *22*, 77−79.
(5) Fried, J. R.; Liu, H. C.; Zhang, C. *J. Polym. Sci., Polym. Lett.* **1989**, *27*, 385−392.
(6) Houde, A. Y.; Kulkarni, S. S.; Kulkarni, M. G. *J. Membr. Sci.* **1992**, *71*, 117−128.
(7) Wind, J. D.; Sirard, S. M.; Paul, D. R.; Green, P. F.; Johnston, K. P.; Koros, W. J. *Macromolecules* **2003**, *36*, 6433−6441.
(8) Fleming, G. K.; Koros, W. J. *Macromolecules* **1986**, *19*, 2285−2291.
(9) Fleming, G. K.; Koros, W. J. *J. Polym. Sci., Polym. Phys.* **1990**, *28*, 1137−1152.
(10) Horn, N. R.; Paul, D. R. *Macromolecules* **2012**, *45*, 2820−2834.
(11) Chiou, J. S.; Paul, D. R. *J. Membr. Sci.* **1987**, *32*, 195−205.
(12) Wessling, M.; Schoeman, S.; van der Boomgaard, T.; Smolders, C. A. *Gas Sep. Purif.* **1991**, *5*, 222−228.
(13) Wessling, M.; Huisman, I.; Vanderboomgaard, T.; Smolders, C. A. *J. Appl. Polym. Sci.* **1995**, *58*, 1959−1966.
(14) Sanders, E. S. *J. Membr. Sci.* **1988**, *37*, 63−80.
(15) Sanders, E. S.; Jordan, S. M.; Subramanian, R. *J. Membr. Sci.* **1992**, *74*, 29−36.
(16) Okamoto, K.; Tanaka, K.; Shigematsu, T.; Kita, H.; Nakamura, A.; Kusuki, Y. *Polymer* **1990**, *31*, 673−678.
(17) Du, N. Y.; Park, H. B.; Dal-Cin, M. M.; Guiver, M. D. *Energy Environ. Sci.* **2012**, *5*, 7306−7322.
(18) Xiao, Y.; Low, B. T.; Hosseini, S. S.; Chung, T. S.; Paul, D. R. *Prog. Polym. Sci.* **2009**, *34*, 561−580.
(19) Staudt-Bickel, C.; Koros, W. J. *J. Membr. Sci.* **1999**, *155*, 145−154.
(20) Kim, J. H.; Koros, W. J.; Paul, D. R. *J. Membr. Sci.* **2006**, *282*, 32−43.
(21) Qiu, W.; Chen, C.-C.; Xu, L.; Cui, L.; Paul, D. R.; Koros, W. J. *Macromolecules* **2011**, *44*, 6046−6056.
(22) Swaidan, R.; Ma, X. H.; Litwiller, E.; Pinnau, I. *J. Membr. Sci.* **2013**, *447*, 387−394.
(23) Park, H. B.; Jung, C. H.; Lee, Y. M.; Hill, A. J.; Pas, S. J.; Mudie, S. T.; Van Wagner, E.; Freeman, B. D.; Cookson, D. J. *Science* **2007**, *318*, 254−258.
(24) Vu, D. Q.; Koros, W. J.; Miller, S. J. *Ind. Eng. Chem. Res.* **2002**, *41*, 367−380.
(25) Vu, D. Q.; Koros, W. J.; Miller, S. J. *Ind. Eng. Chem. Res.* **2003**, *42*, 1064−1075.
(26) Vu, D.; Koros, W. J.; Miller, S. J. *J. Membr. Sci.* **2003**, *221*, 233−239.
(27) Bos, A.; Punt, I. G. M.; Wessling, M.; Strathmann, H. *Sep. Purif. Technol.* **1998**, *14*, 27−39.
(28) Duthie, X.; Kentish, S.; Pas, S. J.; Hill, A. J.; Powell, C.; Nagai, K.; Stevens, G.; Qiao, G. *J. Polym. Sci., Polym. Phys.* **2008**, *46*, 1879−1890.
(29) Das, M.; Koros, W. J. *J. Membr. Sci.* **2010**, *365*, 399−408.
(30) Vaughn, J. T.; Koros, W. J.; Johnson, J. R.; Karvan, O. *J. Membr. Sci.* **2012**, *401*−*402*, 163−174.

(31) Kawakami, H.; Mikawa, M.; Nagaoka, S. *J. Membr. Sci.* **1996**, *118*, 223−230.
(32) Vaughn, J.; Koros, W. J. *Macromolecules* **2012**, *45*, 7036−7049.
(33) Hirayama, Y.; Yoshinaga, T.; Kusuki, Y.; Ninomiya, K.; Sakakibara, T.; Tamari, T. *J. Membr. Sci.* **1996**, *111*, 183−192.
(34) Swaidan, R.; Ghanem, B. S.; Litwiller, E.; Pinnau, I. *J. Membr. Sci.* **2014**, *457*, 95−102.
(35) Ma, X. H.; Swaidan, R.; Belmabkhout, Y.; Zhu, Y. H.; Litwiller, E.; Jouiad, M.; Pinnau, I.; Han, Y. *Macromolecules* **2012**, *45*, 3841−3849.
(36) Qiu, W. L.; Xu, L. R.; Chen, C. C.; Paul, D. R.; Koros, W. J. *Polymer* **2013**, *54*, 6226−6235.
(37) Puleo, A. C.; Paul, D. R.; Kelley, S. S. *J. Membr. Sci.* **1989**, *47*, 301−332.
(38) Kamide, K.; Okajima, K.; Saito, M. *Polym. J.* **1981**, *13*, 115−125.
(39) Fried, J. R.; Li, W. *J. Appl. Polym. Sci.* **1990**, *41*, 1123−1131.
(40) Chern, R. T.; Koros, W. J.; Sanders, E. S.; Yui, R. *J. Membr. Sci.* **1983**, *15*, 157−169.
(41) McKeown, N. B. *ISRN Mater. Sci.* **2012**, *2012*, 16.
(42) McKeown, N. B.; Budd, P. M. *Chem. Soc. Rev.* **2006**, *35*, 675−683.
(43) Budd, P. M.; McKeown, N. B. *Polym. Chem.* **2010**, *1*, 63−68.
(44) Budd, P. M.; Ghanem, B. S.; Makhseed, S.; McKeown, N. B.; Msayib, K. J.; Tattershall, C. E. *Chem. Commun.* **2004**, 230−231.
(45) Carta, M.; Croad, M.; Malpass-Evans, R.; Jansen, J. C.; Bernardo, P.; Clarizia, G.; Friess, K.; Lanč, M.; McKeown, N. B. *Adv. Mater.* **2014**, *26*, 3526−3531.
(46) Ghanem, B. S.; Swaidan, R.; Litwiller, E.; Pinnau, I. *Adv. Mater.* **2014**, *26*, 3688−3692.
(47) Swaidan, R.; Al-Saeedi, M.; Ghanem, B.; Litwiller, E.; Pinnau, I. *Macromolecules* **2014**, *47*, 5104−5114.
(48) Ghanem, B. S. *Polym. Chem.* **2012**, *3*, 96−98.
(49) Ghanem, B. S.; Swaidan, R.; Ma, X.; Litwiller, E.; Pinnau, I. *Adv. Mater.* **2014**, DOI: 10.1002/adma.201401328.
(50) Carta, M.; Malpass-Evans, R.; Croad, M.; Rogan, Y.; Jansen, J. C.; Bernardo, P.; Bazzarelli, F.; McKeown, N. B. *Science* **2013**, *339*, 303−307.
(51) Rogan, Y.; Malpass-Evans, R.; Carta, M.; Lee, M.; Jansen, J. C.; Bernardo, P.; Clarizia, G.; Tocci, E.; Friess, K.; Lanc, M.; McKeown, N. B. *J. Mater. Chem. A* **2014**, *2*, 4874−4877.
(52) Robeson, L. M. *J. Membr. Sci.* **2008**, *320*, 390−400.
(53) Koros, W. J.; Walker, D. R. B. *Polym. J.* **1991**, *23*, 481−490.
(54) Du, N. Y.; Park, H. B.; Robertson, G. P.; Dal-Cin, M. M.; Visser, T.; Scoles, L.; Guiver, M. D. *Nat. Mater.* **2011**, *10*, 372−375.
(55) Weber, J.; Su, O.; Antonietti, M.; Thomas, A. *Macromol. Rapid Commun.* **2007**, *28*, 1871−1876.
(56) Ritter, N.; Senkovska, I.; Kaskel, S.; Weber, J. *Macromolecules* **2011**, *44*, 2025−2033.
(57) Weber, J.; Schmidt, J.; Thomas, A.; Bohlmann, W. *Langmuir* **2010**, *26*, 15650−15656.
(58) O'Brien, K. C.; Koros, W. J.; Barbari, T. A.; Sanders, E. S. *J. Membr. Sci.* **1986**, *29*, 229−238.
(59) Wachsman, E. D.; Frank, C. W. *Polymer* **1988**, *29*, 1191−1197.
(60) Hasegawa, M.; Kochi, M.; Mita, I.; Yokota, R. *Eur. Polym. J.* **1989**, *25*, 349−354.
(61) Budd, P. M.; McKeown, N. B.; Fritsch, D. *J. Mater. Chem.* **2005**, *15*, 1977−1986.
(62) Ilinitch, O. M.; Fenelonov, V. B.; Lapkin, A. A.; Okkel, L. G.; Terskikh, V. V.; Zamaraev, K. I. *Microporous Mesoporous Mater.* **1999**, *31*, 97−110.
(63) Guiver, M. D.; Lee, Y. M. *Science* **2013**, *339*, 284−285.
(64) Tanaka, K.; Okano, M.; Toshino, H.; Kita, H.; Okamoto, K. I. *J. Polym. Sci., Polym. Phys.* **1992**, *30*, 907−914.
(65) Maier, G. *Angew. Chem., Int. Ed.* **2013**, *52*, 4982−4984.
(66) Pinnau, I.; Toy, L. G. *J. Membr. Sci.* **1996**, *116*, 199−209.
(67) Thomas, S.; Pinnau, I.; Du, N. Y.; Guiver, M. D. *J. Membr. Sci.* **2009**, *333*, 125−131.
(68) Bos, A.; Punt, I. G. M.; Wessling, M.; Strathmann, H. *J. Membr. Sci.* **1999**, *155*, 67−78.
(69) Robeson, L. M.; Smith, Z. P.; Freeman, B. D.; Paul, D. R. *J. Membr. Sci.* **2014**, *453*, 71−83.
(70) Hirose, T.; Mi, Y.; Stern, S. A.; Stclair, A. K. *J. Polym. Sci., Polym. Phys.* **1991**, *29*, 341−347.
(71) Horn, N. R.; Paul, D. R. *Polymer* **2011**, *52*, 5587−5594.
(72) Budd, P. M.; McKeown, N. B.; Ghanem, B. S.; Msayib, K. J.; Fritsch, D.; Starannikova, L.; Belov, N.; Sanfirova, O.; Yampolskii, Y.; Shantarovich, V. *J. Membr. Sci.* **2008**, *325*, 851−860.
(73) Wessling, M.; Lopez, M. L.; Strathmann, H. *Sep. Purif. Technol.* **2001**, *24*, 223−233.
(74) Li, P.; Chung, T. S.; Paul, D. R. *J. Membr. Sci.* **2013**, *432*, 50−57.
(75) White, L. S.; Blinka, T. A.; Kloczewski, H. A.; Wang, I. F. *J. Membr. Sci.* **1995**, *103*, 73−82.
(76) Kim, T. H.; Koros, W. J.; Husk, G. R.; Obrien, K. C. *J. Membr. Sci.* **1988**, *37*, 45−62.
(77) Jordan, S. M.; Fleming, G. K.; Koros, W. J. *J. Polym. Sci., Polym. Phys.* **1990**, *28*, 2305−2327.